White paper

MR-based Synthetic CT reimagined

An AI-based algorithm for continuous Hounsfield units in the pelvis and brain – with *syngo*.via RT Image Suite (VB60)

siemens-healthineers.com/radiotherapy

Michaela Hoesl, PhD

Nuria Escobar Corral, PhD

Nilesh Mistry, PhD

SIEMENS Healthineers

MR-based Synthetic CT for an MR-only workflow

MR-based Synthetic CT offers the possibility of combining the superior soft-tissue contrast of MRI for organ at risk and target delineation with dosimetric planning. An MR-only workflow eliminates the need for CT to MRI registration, reducing systematic registration errors and unnecessary ionizing radiation from CT scans. Our latest solution for MR-only workflows[1] includes an AI-based algorithm for generating Synthetic CT images from MRI for pelvis and brain.

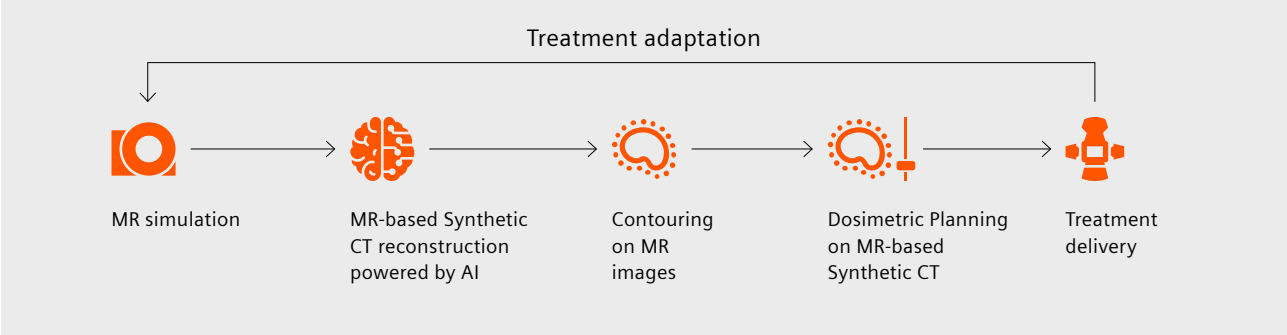

MR-only workflow

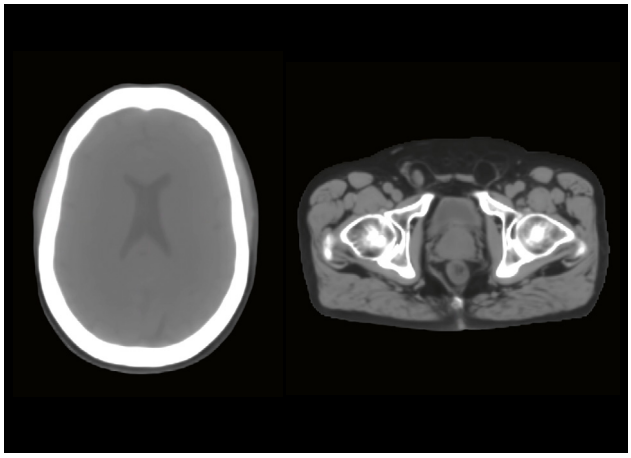

Key features:

- Geometric fidelity
- Continuous Hounsfield units
- Three different outputs are available: 120 kV equivalent, electron density, and mass density images
- DICOM format
- For brain and male/female pelvis
- In-plane resolution of 1 mm x 1 mm (brain), 2 mm x 2 mm (pelvis)

Clinical evaluation

Brain: Universitätsklinikum Erlangen, Germany

- < 1% mean dose difference in PTV, GTV, evaluated OAR
- < 0.5% and 1.4% mean dose difference for the brainstem and chiasma respectively

Pelvis: Brigham & Women's Hospital, Dana-Farber Cancer Institute, Harvard Medical School, Boston, USA

- < 1% dose difference in the CTV, evaluated OAR
- 1% / 2 mm gamma analysis showed mean agreement of 98.9 ± 0.3%
- Spatial positioning evaluation with CBCT < 1 mm absolute differences in x-, y-, and z-direction

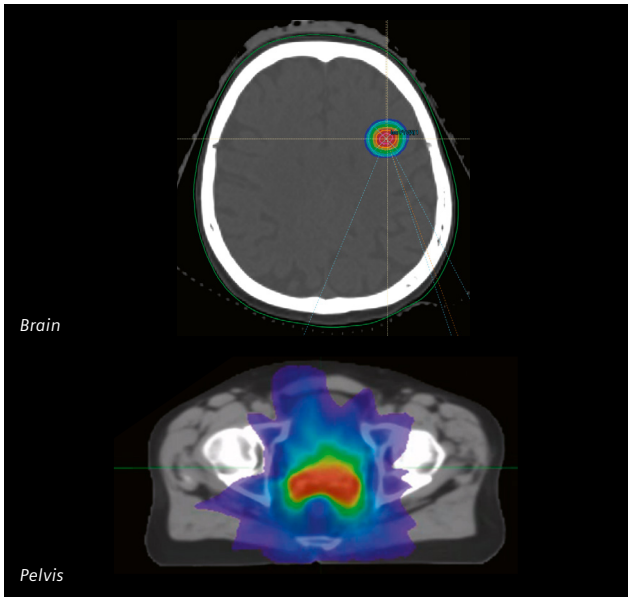

[1] *Since syngo.via RTiS VB60*

Benefits of MR-based Synthetic CT for an MR-only workflow

Clinical benefits

- Supports MR as the primary imaging modality for RT treatment preparation of brain and pelvic cancer patients
- Offers dedicated sequences to achieve soft-tissue contrast for organ-at-risk and target delineation[1]
- Eliminates the need to register between CT and MR for treatment planning helping to avoid registration errors[2,3,4]
- Eliminates unnecessary ionizing radiation from CT imaging

Operational benefits

Simplifies the workflow:

- Offers a CT-free, straightforward workflow for target definition, patient marking, and beam placement on DRR
- Decreases the number of scans required and associated patient inconvenience[5]
- Enables generation of density information for further dose calculations in the TPS*
- Enables the use of a single calibration curve** in the TPS independent of modalities with the generation of mass and electron density maps

Financial benefits

- AI-based algorithm helps maximize MR-only workflow efficiency with reconstruction from a single MRI scan
- MR-only workflow eliminates the need for CT simulation, freeing up the CT scanner for other patients

[1] *Kashani R, Olsen JR. Magnetic Resonance Imaging for Target Delineation and Daily Treatment Modification. Semin Radiat Oncol. 2018; 28(3): 178–184.*
[2] *Roberson PL, McLaughlin PW, Narayana V, Troyer S, Hixson GV, Kessler ML. Use and uncertainties of mutual information for computed tomography/ magnetic resonance (CT/MR) registration post permanent implant of the prostate. Med Phys. 2005; 32(2): 473–82.*
[3] *Dean CJ, Sykes JR, Cooper RA, Hatfield P, Carey B, Swift S, et al. An evaluation of four CT-MRI co-registration techniques for radiotherapy treatment planning of prone rectal cancer patients. Br J Radiol. 2012; 85(1009): 61–68.*
[4] *Nyholm T, Nyberg M, Karlsson MG, Karlsson M. Systematisation of spatial uncertainties for comparison between a MR and a CT-based radiotherapy workflow for prostate treatments. Radiat Oncol. 2009; 4: 54.*
[5] *Karlsson M, Karlsson MG, Nyholm T, Amies C, Zackrisson B. Dedicated magnetic resonance imaging in the radiotherapy clinic. Int J Radiat Oncol Biol Phys. 2009; 74(2): 644–51.*
** Treatment planning system (TPS)*
*** When used along with DirectDensity. DirectDensity is a reconstruction available for CT. For more information see: Whitepaper DirectDensity. Technical Principles and implications for radiotherapy.*

Why MRI in radiotherapy?

Radiotherapy treatment simulation and planning are conventionally performed on computed tomography (CT) images because of the intrinsic relationship between Hounsfield units (HU) and electron density information, needed to model radiation attenuation in the treatment planning system [1]. Compared with CT images, MRI shows superior soft-tissue contrast (Figure 1) and is becoming the modality of choice for delineation of target organs and organs at risk (OAR) [2]. Moreover, MRI gives access to multiparametric data, such as T1w, T2w, dynamic contrast-enhanced MRI (DCE-MRI), and diffusion-weighted imaging (DWI) [3–7], which play an increasingly important role in the whole workflow from diagnosis, structure delineation, treatment planning, and response assessment.

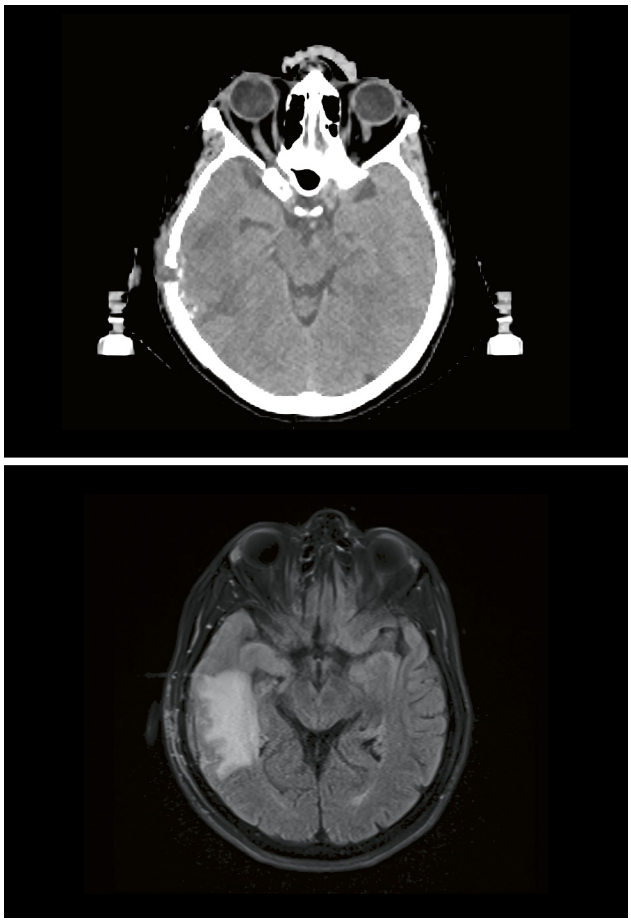

Figure 1: Left image: CT, right image: MRI (T2 flair)
Courtesy of Universitätsklinikum Erlangen, Germany.

Dose calculation

Dose calculation requires a 3D electron or mass density map and unfortunately the necessary correlation between the nuclear magnetic properties and electron density is missing. Therefore, MR images cannot directly be used for dose calculation. When MR images are used for contouring, a CT image is required for dose calculation, resulting in a combined MRI-CT workflow.

Main challenge of a combined MRI-CT workflow

In multimodality workflows, rigid and sometimes deformable image registration (DIR) are employed. When anatomies deviate significantly (bladder filling or rectal filling, Figure 2) fusing of CT and MRI modalities becomes difficult and adds to uncertainties in the planning process [8, 9].

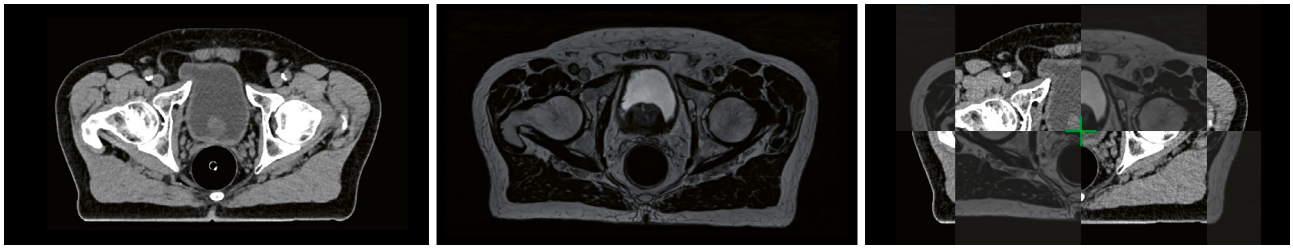

Figure 2: Left image: Planning CT, center image: T2w MRI, right image: registration visualized with the checkerboard tool[1].
Registration errors may persist and registration can be cumbersome.
Courtesy of Universitätsklinikum Erlangen, Germany.

[1] *Since syngo.via RTiS VB60*

MR-only workflow for the pelvis and brain

The MAGNETOM Sola (1.5T) and MAGNETOM Vida (3T)[1] are our MRI systems supporting MR-only workflows. Both MAGNETOM RT Pro edition systems are dedicated to RT with continuous development and updates with the latest features for RT simulation:

- Reproducible patient positioning with MR-compatible, certified, and indexed flat tabletop overlays, immobilization devices, and an external laser bridge
- Flexible coils with multiple channels
- RT Dot Engine with dedicated RT protocols including workflow guidance
- Automatic, optimal (2D/3D) distortion correction for spatial integrity for robustness and reproducibility
- QA solutions including an in-depth guide: QA cookbook [10]
- MR-based Synthetic CT with continuous HU

An example of an MR-only workflow protocol for pelvis is shown in Figure 3. The key sequence for MR-based Synthetic CT reconstruction, the T1 VIBE-Dixon sequence, follows the optional T1w and T2w clinical sequences for morphological information precontrast and postcontrast. Additional sequences, such as, for example diffusion-weighted images (DWI), can be acquired to obtain further insights and support target definition. [18]

Advanced sequences like DWI can potentially be used for treatment response evaluation. [11]

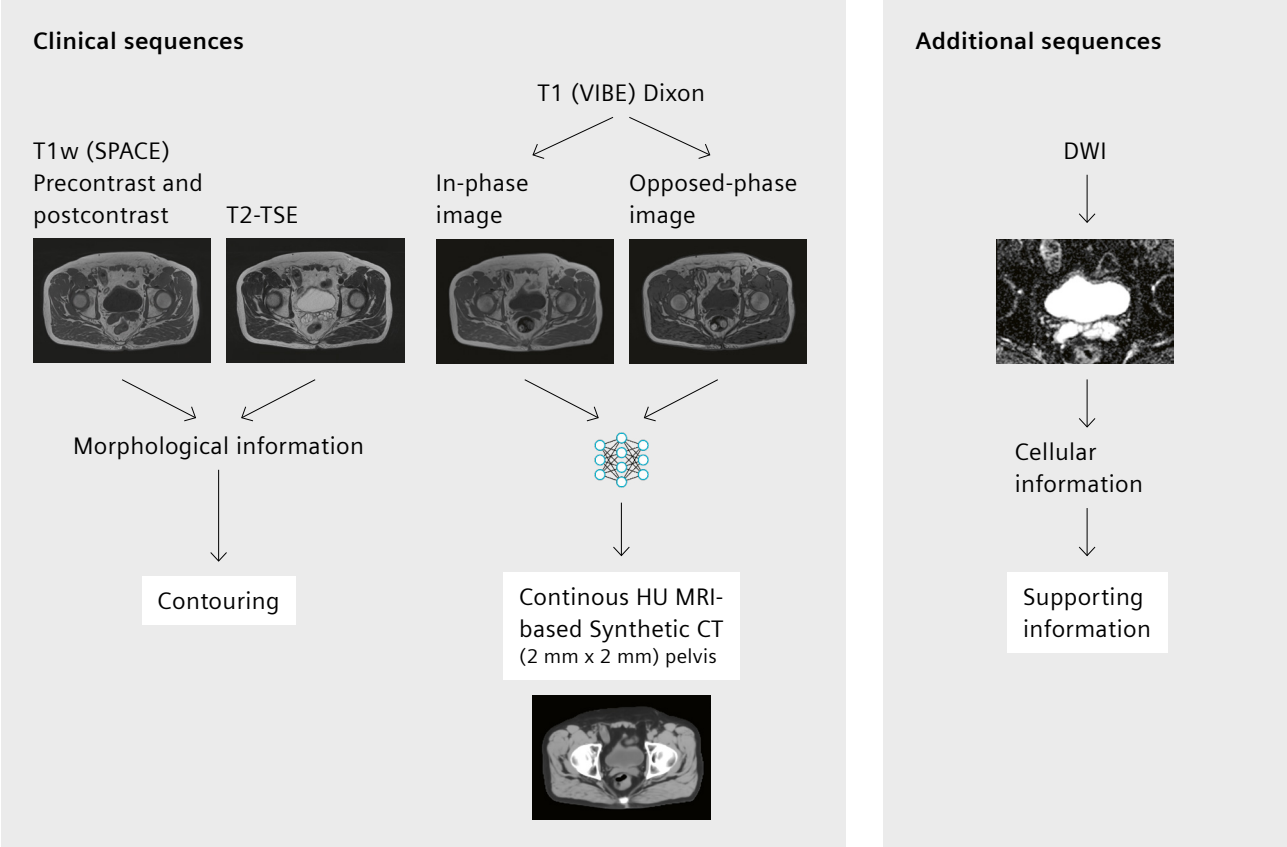

Figure 3: Example of a scanning protocol for a prostate MR-only workflow.
Courtesy of Universitätsklinikum Erlangen, Germany

[1] *The data acquisition protocols for Synthetic CT are available with syngo MR XA11A and later software versions with MAGNETOM RT Pro edition for MAGNETOM Vida and MAGNETOM Sola, with syngo XA30 and later software Versions for MAGNETOM Aera and MAGNETOM Skyra.*

MR-based Synthetic CT generation algorithm – How does it work?

In recent years, the field of MR-based Synthetic CT imaging has gained substantial interest [12–17]. Different methods have been proposed so far to create electron density information from MRI artificially [15, 18]. Our latest algorithm for MR-based Synthetic CT is an AI-based algorithm. The model was trained by leveraging deep learning (DL) neural network technology. The DL algorithm uses a combination of multilayer neural networks to learn Synthetic CT reconstruction. Training was accomplished using a large number of datasets for training with 6486 CT and MRI image pairs for brain and 9059 for pelvis (validation sets were 553 for brain and 695 for pelvis). For the training image pairs, CT images were registered to MRI using rigid and deformable registration. The input for the trained deep learning algorithm are only the VIBE-Dixon in-phase and opposed-phase images for Synthetic CT reconstruction. The AI-based Synthetic CT product comes fully trained to the user and does not continue training at the user's site.

The network architecture (Figure 4) consists of two parts: **Network 1: convolutional neural network** (densely connected UNet) for segmentation in three classes: background, bone, and soft tissue from a two-channel input using the MR images.

Network 2: generator and discriminator (conditional GAN) for Synthetic CT reconstruction with continuous HU (one output channel). During training, the input and condition are the MR images concatenated with the segmentation results of the first network (five input channels) to guide the training of the conditional GAN.

- Generator (densely connected UNet): receives a five-channel input (in-phase, opposed-phase Dixon MRI and the segmentation output in three tissue classes) for Synthetic CT reconstruction.
- Discriminator: tries to discriminate the prediction of the generator (Synthetic CT) from the ground truth (real CT image). During training, the information is fed back iteratively to yield a machine-generated Synthetic CT, which is indistinguishable from a real CT image.

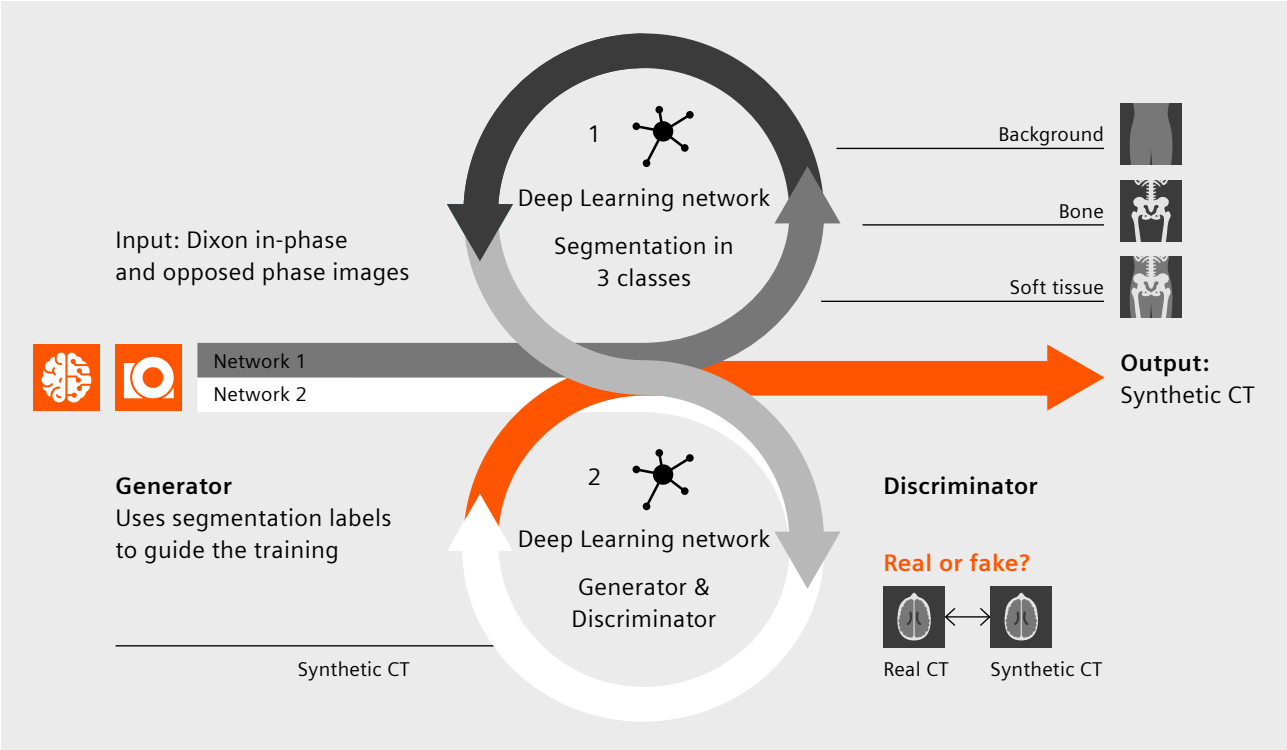

Figure 4: The cGAN (conditional generative adversarial network) training scheme.

VIBE Dixon acquisition for MR-based Synthetic CT reconstruction

T1 VIBE Dixon	1.5T acquisition time	Resolution	3T acquisition time	Resolution
Head	3 min 25 s	1.5x1.5x1.5 mm^3	2 min 22 s	1.3x1.3x1.0 mm^3
Pelvis	2 min 21 s	2.0x2.0x2.0 mm^3	1 min 33 s	2.0x2.0x2.0 mm^3
	4 min 12 s	1.6x1.6x2.0 mm^3	2 min 48 s	1.6x1.6x2.0 mm^3

Table 1: T1 VIBE-Dixon sequence with example acquisition time and image resolution at 1.5T and 3T for brain and pelvis: For pelvis, the acceleration mode CAIPIRINHA [18] was selected with a total acceleration factor of 4–5. For the brain at 1.5T, no acceleration mode was used. At 3T, GRAPPA [19] with a total acceleration factor of 2 was selected.

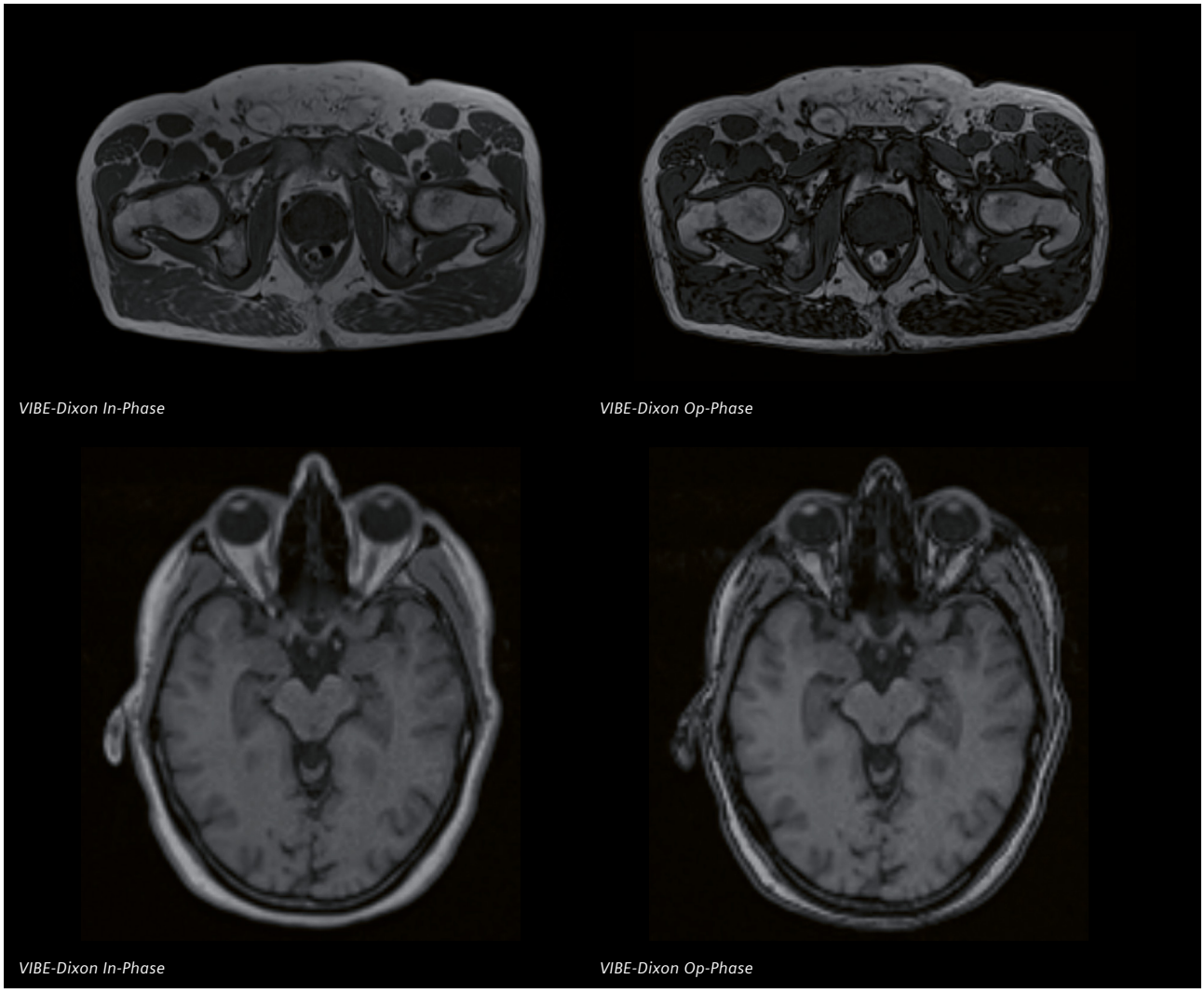

Figure 5: VIBE-Dixon in-phase and opposed-phase images of a male pelvis and brain.
Courtesy of Siemens Healthineers, Erlangen, Germany

MR scanning parameters for the VIBE-Dixon sequence as input for Synthetic CT reconstruction are automatically handled in the RT Dot Engine.

In the RT Dot Engine, axial orientation reformatting and distortion correction are automatically preselected. The neural network imposes certain requirements on the input data. The network expects MR volume pairs in axial orientation. Therefore, volumes are always reformatted to axial orientation. The fully trained network requires input images with dimensions (in x-axis and y-axis) in multiples of 16, which is also pre-selected in the RT Dot Engine. Otherwise, zero padding is performed before the synthesis. Additionally, input images need 98th percentile normalizations, which is done automatically in the postprocessing pipeline.

The resulting Synthetic CT has an in-plane resolution of 1 mm x 1 mm (brain) and 2 mm x 2 mm (pelvis). The slice thickness is determined by the acquired input data.

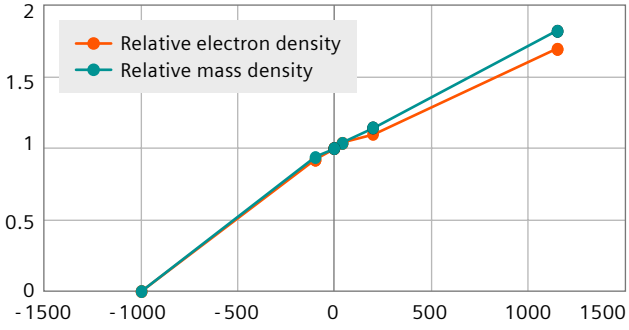

Figure 6: Synthetic CT calibration curve

Synthetic CT import in the treatment planning system

The generated MR-based Synthetic CT image can be exported in HU, relative electron density (RED), and relative mass density (RMD). When exported as HU, for dose calculation the HU values of the synthetic CT have to be converted to RED or RMD in the TPS. For this purpose, the following table can be used. If RED and RMD are chosen as output, the calibration table is automatically applied by the software. The MR-based Synthetic CT image is labeled in DICOM as "CT" and is therefore recognized by the TPS and LINAC as a CT image.

Tissue class	HU value	Relative electron density	Relative mass density
Air	-1000	0	0
Fat	-100	0.924	0.941
Liquid	0	1	1
Brain/Muscle	40	1.04	1.04
Spongeous Bone	200	1.096	1.143
Cortical Bone	1150	1.695	1.823

MR-based Synthetic CT results for pelvis and brain

In Figure 7, an example of the results obtained for pelvis and brain are shown. Both the soft-tissue window level and bone window level are presented. Besides dose planning, Synthetic CT can be used to verify the patient's position on the LINAC by matching the Synthetic CT with the cone-beam CT or the 2D synthetic DRR (derived from the Synthetic CT) with the flat-panel radiograph (Figure 8).

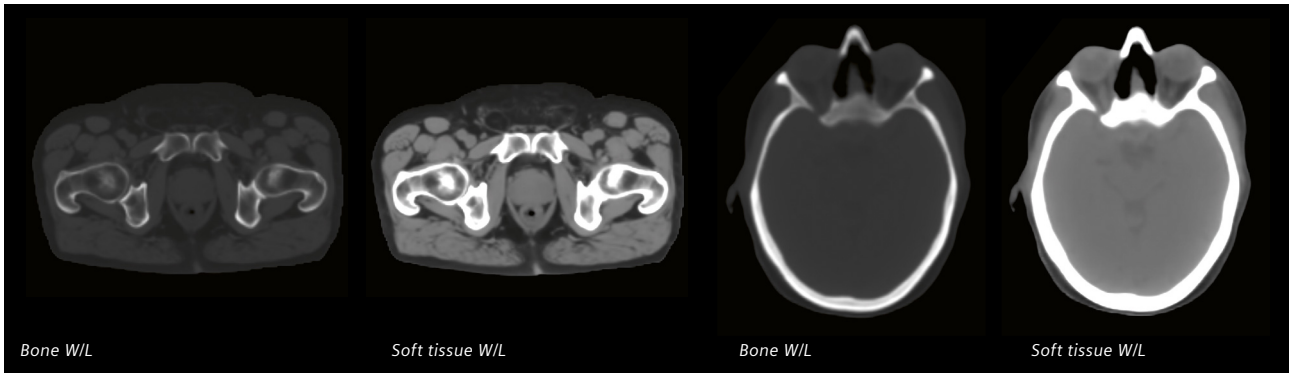

Figure 7: Synthetic CT for the pelvis and brain in two different window levels (W/L): bone and soft tissue.
Courtesy of Siemens Healthineers, Erlangen, Germany

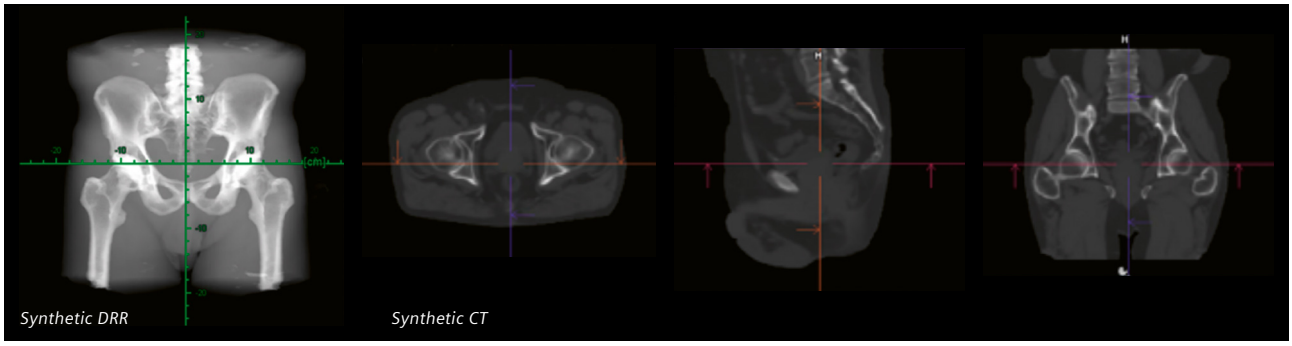

Figure 8: Synthetic DRR for matching with DRR and Synthetic CT for matching with cone-beam CT images for patient positioning.
Courtesy of Siemens Healthineers, Erlangen, Germany

Evaluation of geometric fidelity and CT number accuracy

We performed an internal validation of geometric fidelity and HU unit accuracy. The geometric fidelity test was passed for both brain and pelvis with an average symmetric surface distance (ASSD) of less than 1 mm (0.9 ± 0.1 mm pelvis, 0.8 ± 0.1 mm brain), which is below the in-plane pixel resolution of 1 mm (2 mm) for the brain (pelvis) and therefore negligible. For HU accuracy, line profiles from CT and MR-based Synthetic CT from the same patient were compared. An example of this comparison is shown in Figure 9. In addition to that, the HU values of the MR-based Synthetic CT were evaluated in multiple 2D regions of interest (ROI) of the tissue types: fat, liquid, soft tissue, and bone and were each compared with the expected literature values. All values, including deviations, fell within the expected range and tolerance (Table 2).

For visual inspection of geometric accuracy, *syngo*.via RTiS VB 60 provides a checkerboard tool (Figure 11a). The HU can be verified in regions of interest using the ROI tool, see Figure 11b.

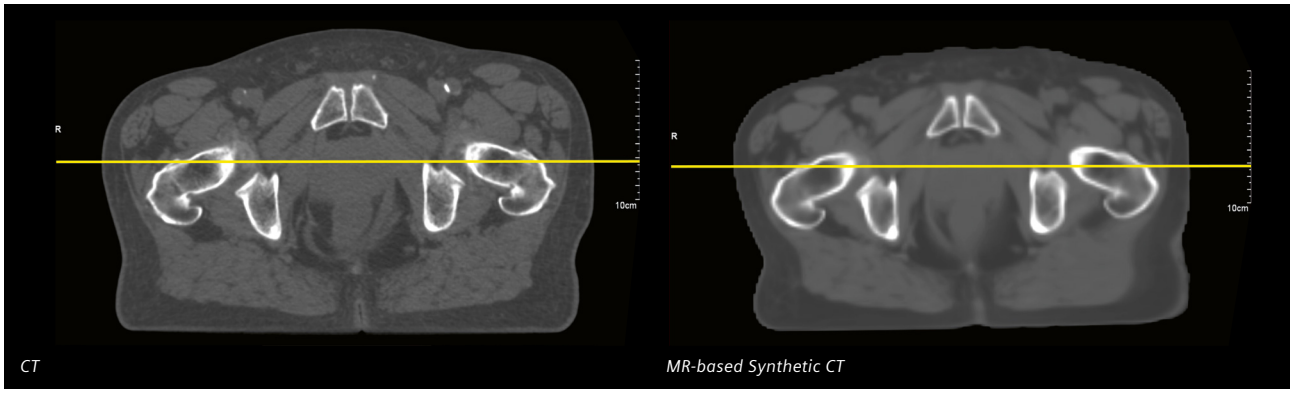

Figure 9: Left image: Planning CT, right image: MR-based Synthetic CT and graph comparing HU along the line profile (yellow lines).
Courtesy of Centre Hospitalier de l'Université de Montréal – CHUM, Montreal, Canada

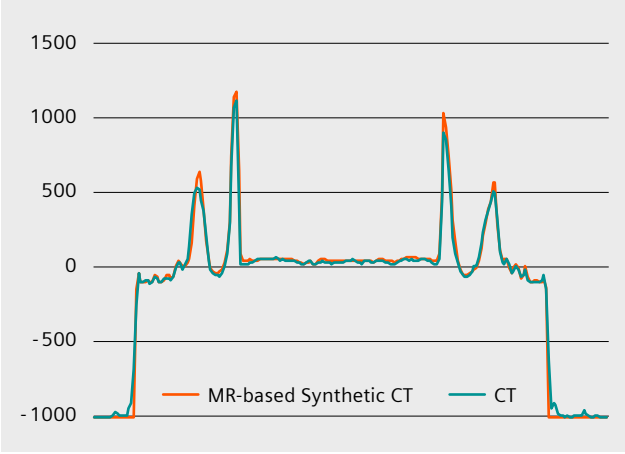

Figure 10: Line profile comparison

ROI	Reference values[1]	Measured in brain	Measured in pelvis
Fat	-100 ± 50	-59 ± 4	-97 ± 1
Liquid (ventricles, bladder)	0 ± 50	7 ± 1	8 ± 2
Soft tissue (brain, muscle)	40 ± 50	27 ± 1	44 ± 2
Cortical bone (skull, femoral head)	1150 ± 200	1103 ± 59	1236 ± 17
Spongeous bone (femoral shaft)	200 ± 200	–	277 ± 9

Table 2: Hounsfield unit (HU) comparison of the MR-based Synthetic CT in multiple regions of interest (ROI) of different tissue types with expected literature values.

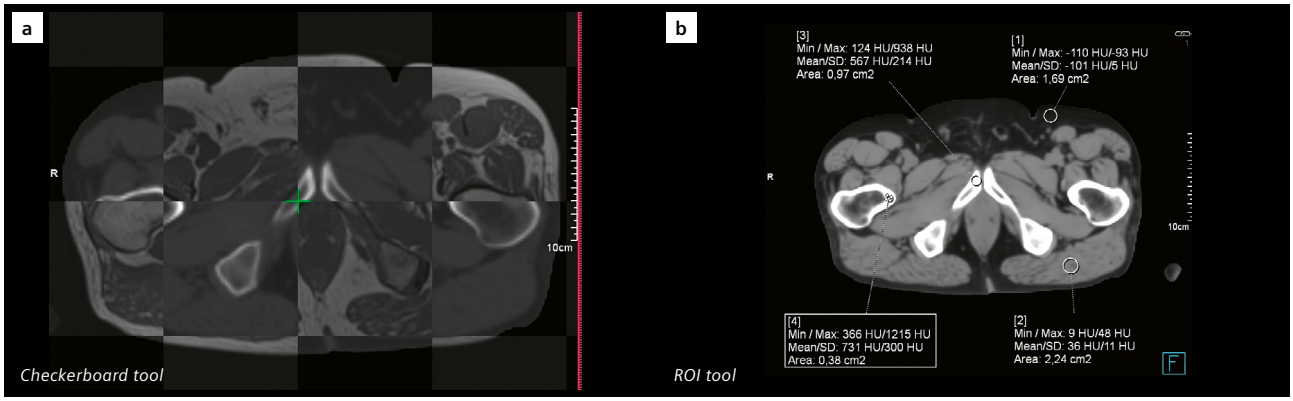

Figure 11: Geometric accuracy and HU value verification with checkerboard inspection and ROI tool in a pelvic case.

[1] *Reference values match the CT lookup table (Table 1).*

Clinical evaluation

Dose difference evaluation between the CT and Synthetic CT is the crucial metric for radiation therapy. The dosimetric and spatial positioning evaluation of the new algorithm relative to standard CT-based planning was performed by two independent clinical partners.

Summary

1. Evaluation of the pelvic MR-based Synthetic CT from Brigham & Women's Hospital, Dana-Farber Cancer Institute, Harvard Medical School, Boston, USA[1]

Overall, differences between the original dose distribution and the dose recalculated on the Synthetic CT were:

- < 1% dose difference in the CTV and evaluated OAR for the seven prostate patients examined. The mean dose difference (ΔDose = Dose (planning CT) – Dose (registered Synthetic CT)) from the CTV was - 0.21% relative to total dose.
- 1%/2 mm gamma analysis showed mean agreement of 98.9 ± 0.3% (range 98.4–99.3%).

Regarding spatial positioning evaluation, 0.12 mm/ - 0.72 mm/- 0.56 mm differences in x-, y-, and z-direction (range: - 1.8–1.4 mm) between registered Synthetic CT to CBCT registration and planning CT-CBCT registration

2. Evaluation of the brain MR-based Synthetic CT from Universitätsklinikum Erlangen, Germany

The mean dose difference was computed and analyzed for all patients for the target volumes (PTV, GTV) and the evaluated organs at risk (brainstem, chiasma, optical nerves).

- < 1% mean dose difference (normalized to the total planned dose) in all the regions of interest
- < 1% (median 0.06%) mean dose differences of PTV und GTV
- < 0.5% and 1.4% mean dose difference for the brainstem and chiasma respectively

Full evaluation

1. Evaluation of the pelvic MR-based Synthetic CT from Brigham & Women's Hospital, Dana-Farber Cancer Institute, Harvard Medical School, Boston, USA

A total of seven prostate cancer patients scheduled for subsequent EBRT underwent same-day MRI (MAGNETOM Vida 3T) and CT (SOMATOM Confidence) simulation. All patients were clinically planned and treated using their planning CT scanner. Parameters were as follows:

- CT: 0.976 mm x 0.976 mm voxel size, 3 mm slice thickness
- MRI: 336 mm x 448 mm field of view, 2 mm x 2 mm voxel size, 2 mm slice thickness. T1 Vibe-Dixon Synthetic CT protocol sequence
- TPS: Eclipse 15.6
- Treatment technique: 6 MV X-rays using a VMAT (RapidArc)
- Dose prescription: 180 cGy/fr for 44 fractions. Some patients received simultaneous integrated boosts and altered fractionations.

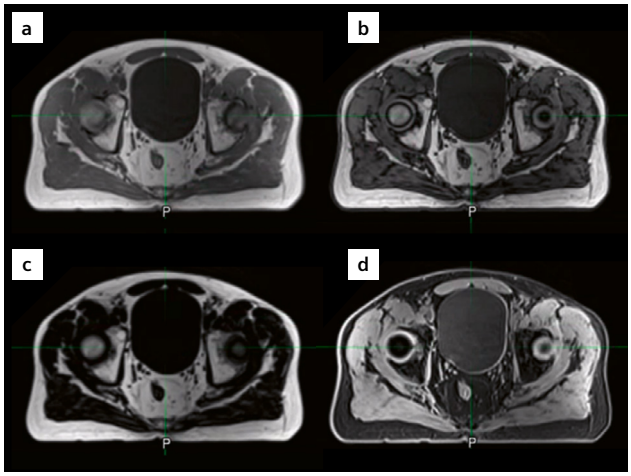

Figure 12: Four MR contrasts generated by the T1 VIBE-Dixon scan protocol (a) in-phase (IP), (b) out-of-phase (OP), (c) fat, (d) water. Only a and b are needed for Synthetic CT postprocessing.

[1] *The clinical evaluation was performed on a prototype; its algorithm does not deviate from the released product.*

Dosimetric accuracy evaluation of the AI-Synthetic CT
MR-based Synthetic CT images were registered to the planning CT (pCT), resampled and then saved into the frame of reference of the pCT. These registered MR-based Synthetic CTs (called "rsCT" in the following) were then imported into the Eclipse treatment planning system. The clinical treatment plans (based on pCT) were copied and recomputed onto the corresponding rsCT using the same plan parameters. Dose differences were computed in OARs (bladder, rectum, and left and right femoral heads) and the CTV prostate target structure. The original contours (from the pCT scans) were used for all subsequent analyses. Dose distributions obtained using the pCT and the rsCT were compared using a 1%/2 mm gamma criteria. [19]

Assessment of spatial localization accuracy (cone-beam CT (CBCT) registration)
Spatial (on treatment) localization accuracy of the Synthetic CT was evaluated by comparing Synthetic CT to CBCT registration results with pCT-CBCT registration in Eclipse/Aria using the Image Registration tool. The first five CBCT scans of each patient were used for this study. Two types of translation-only registrations were performed:

- CBCT scans were registered to the space of the pCT.
- CBCT scans were registered to the space of the rsCT (Synthetic CT registered to the planning CT).

Differences in the translation vectors of the pCT-CBCT registration and rsCT-CBCT registration (e.g., Δx = translation_x(pCT)–translation_x (rsCT)) were calculated and averaged among the five CBCT cases.

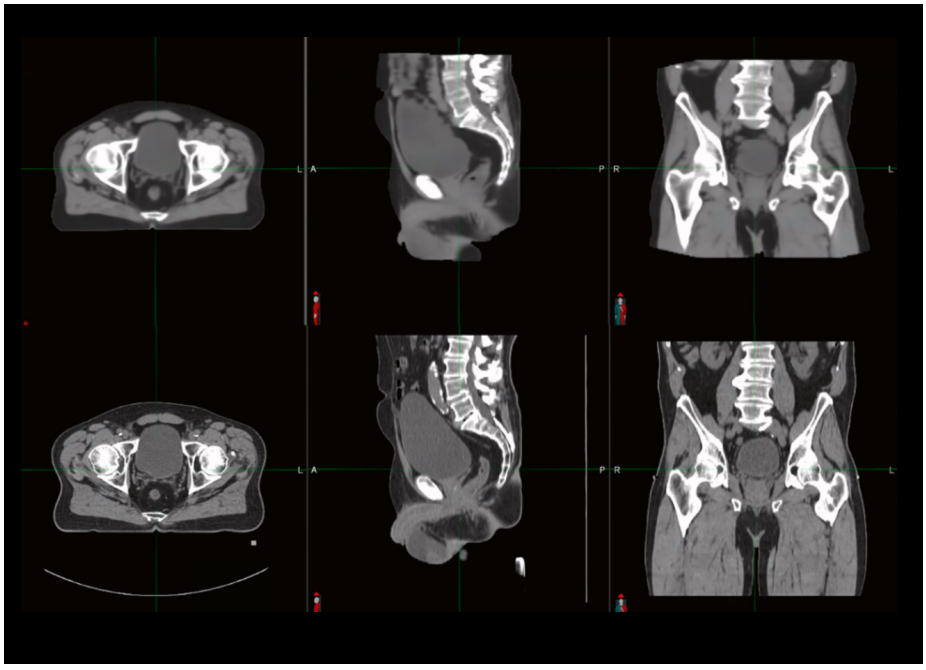

Figure 13: MR-based Synthetic CT (top) compared with conventional planning CT (bottom) of the same patient.

Dosimetric results in the pelvis

Differences between the original dose distribution on the pCT and the recalculated dose distribution on the Synthetic CT were globally < 1% for the seven patients examined. The difference in the dose calculated for the prostate (CTV), penile bulb (when contoured), bladder, rectum, and both femoral heads are tabulated in Table 3. The mean dose difference (ΔDose = Dose (pCT)–Dose (rsCT)) to the CTV was -0.21% relative to the total dose. Results of gamma analysis at 1%/2 mm showed a mean agreement of 98.9 ± 0.3% (range 98.4–99.3%).

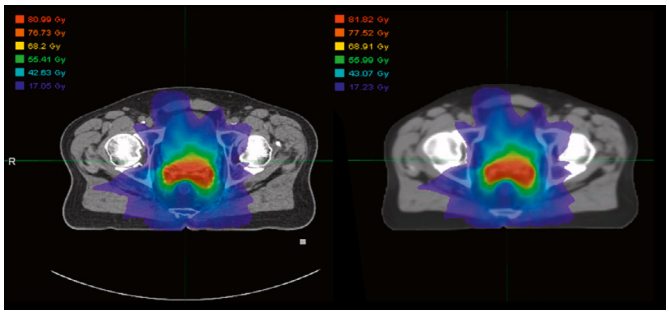

Figure 14: Exemplary dose distributions of a treatment plan calculated on the planning CT (left) and the MR-based Synthetic CT (right).

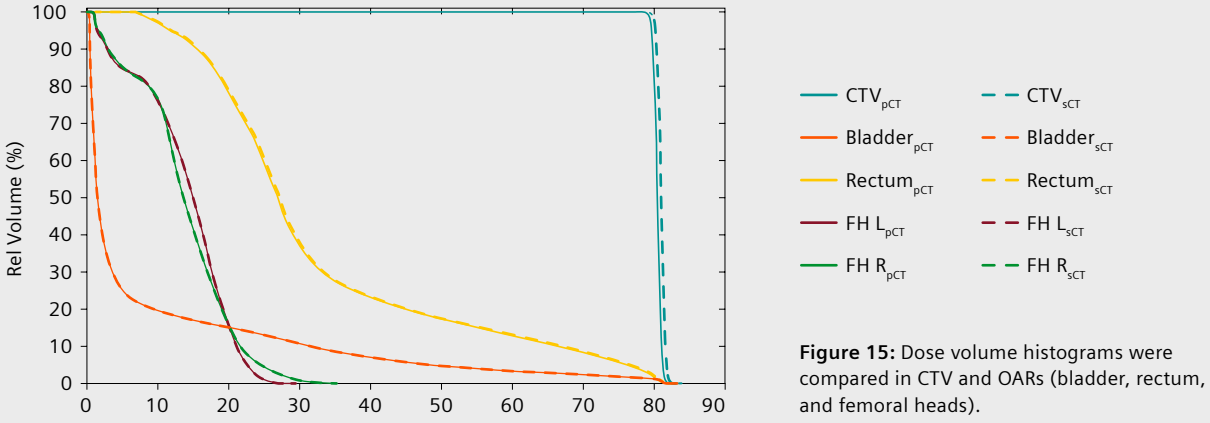

Figure 15: Dose volume histograms were compared in CTV and OARs (bladder, rectum, and femoral heads).

Patient	CTV (% difference)	Bladder (Gy)	Rectum (Gy)	Femoral head left (Gy)	Femoral head right (Gy)	Gamma 1%/2mm
1	-0.62%	-0.05	-0.15	-0.04	-0.08	99.1%
2	0.28%	0.02	-0.05	0.19	0.07	98.4%
3	-0.49%	-0.08	-0.31	0.01	-0.05	98.4%
4	-0.74%	-0.43	-0.62	0.06	0.12	99.2%
5	-0.08%	0.03	-0.33	0.07	0.09	99.3%
6	0.58%	-0.03	-0.13	-0.03	-0.03	99.3%
7	-0.30%	-0.01	-0.05	-0.14	-0.05	98.9%
Mean	-0.21%	-0.078	-0.23	0.017	0.01	98.9%
STD	0.44%	0.16	0.20	0.10	0.08	0.3%

Table 3: Differences in dose distributions of pCT- and Synthetic CT-based dose plans. Dose differences in CTV, PTV, and OAR were calculated as ΔDose = Dose(pCT) - Dose(rsCT).

Spatial localization accuracy results (CBCT registration)

Differences between rsCT-CBCT registration results and pCT-CBCT registration were assessed (Table 4). On average, 0.12 mm/-0.72 mm/-0.56 mm in x-, y-, and z-direction respectively (range: -1.8–1.4 mm) were observed.

Patient	1	2	3	4	5	6	7	Mean	STD
X (mm)	1.4	0.46	0.1	-1.3	0.08	-0.36	0.5	0.12	0.83
Y (mm)	-1.1	-1.06	-0.26	-1.22	-0.14	-1.44	0.2	-0.72	0.63
Z (mm)	-1.02	-1.2	-0.56	1.14	-0.48	0	-1.8	-0.56	0.94

Table 4: Difference in the translation vector (mm) between rsCT-CBCT registration and pCT-CBCT registration. Difference was calculated as translation (pCT)–translation (rsCT) in X, Y, Z axes.

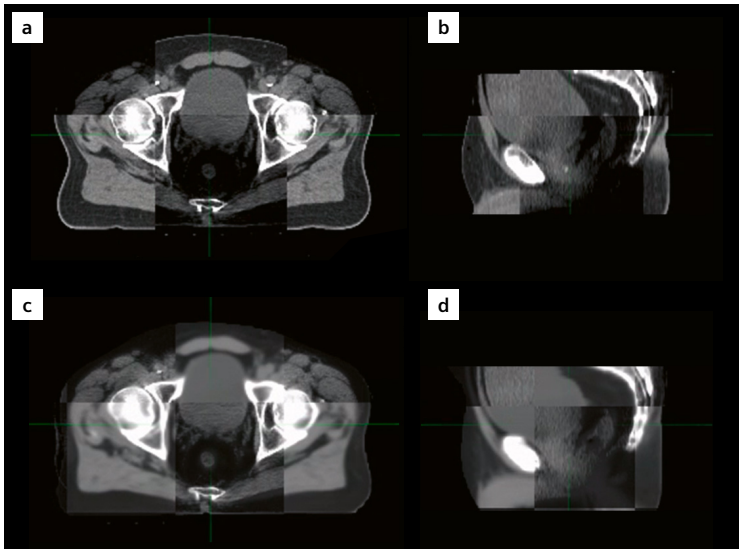

Figure 16: Localization accuracy comparison using the original planning CT data to CBCT registration as the reference (a, b), versus CBCT registration to the MR-based Synthetic CT (c, d).

2. Evaluation of the brain MR-based Synthetic CT from Universitätsklinikum Erlangen, Germany

A total of five brain cancer patients underwent MRI (MAGNETOM Sola 1.5T) and CT (SOMATOM go.Open Pro) simulation with a maximal time delay of five days. Both simulation images were acquired in a dedicated RT setup to minimize differences in the head position between MRI, CT, and RT treatment.

The five patients were scheduled for subsequent EBRT. All patients were treated with 6 MV X-rays using a VMAT (RapidArc) treatment technique with different dose prescriptions. A clinical treatment plan according to institutional clinical guidelines was optimized on the planning CT. The thermoplastic mask structure was removed on the planning CT image to obtain the same body contour as in Synthetic CT. The same plan was recalculated on the Synthetic CT. The mean doses of the target volumes (PTV, GTV) and OARS (brainstem, chiasma, optical nerves) were compared. In all the regions of interest, the mean dose differences were below 1% (normalized to the total planned dose).

The mean dose difference for PTV und GTV were overall below 1%, with a median of 0.06%. For the brainstem and chiasma, the mean dose difference was overall below 0.52% and 1.37% respectively.

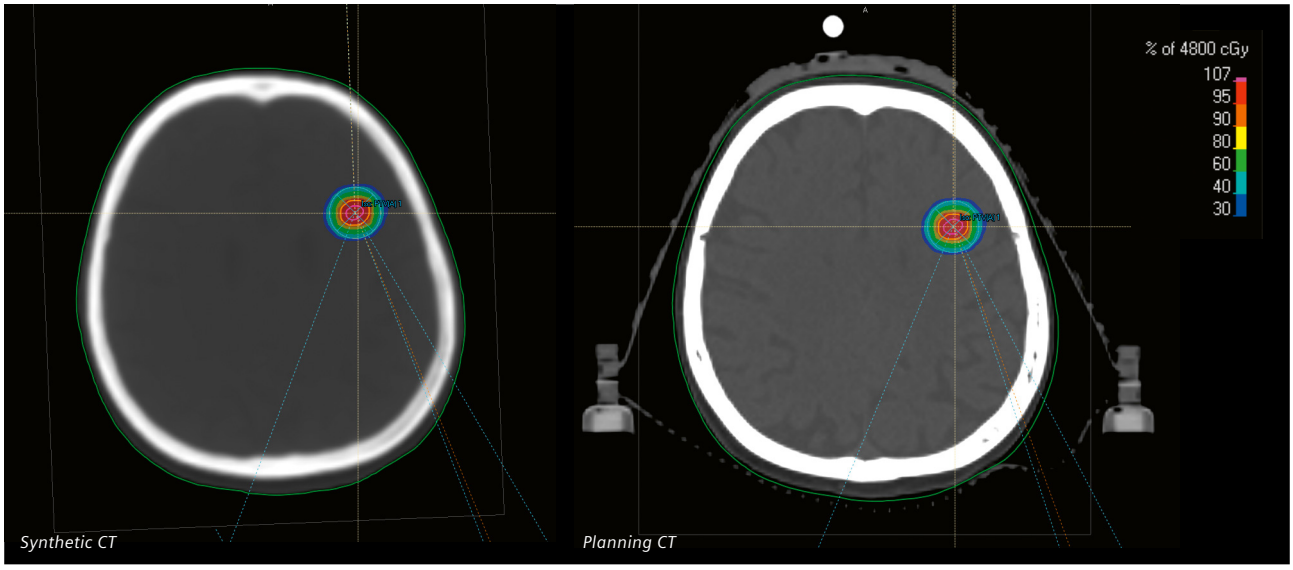

Figure 17: Dose distribution on Synthetic CT and CT with corresponding DVHs

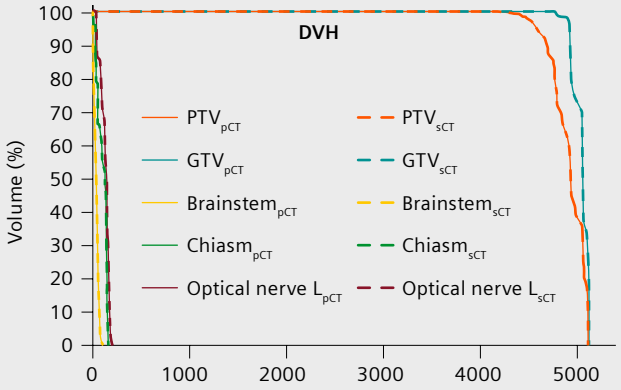

Mean dose [cGy] in ROI	on CT	on sCT
PTV	4919	4914
GTV	5045	5038
Brainstem	34	34
Chiasma	100	100
OPT_NRV_L	125	124
OPT_NRV_R	19	19

Figure 18: Mean dose on the planning CT and Synthetic CT (sCT) in six regions of interest for one patient.

Mean dose difference [%]

Patient	Prescription dose	PTV	GTV	Brainstem	Chiasma
P1	12fx x 4 Gy	-0.10	-0.14	0	0
P2	25fx x 2 Gy	0.08	0.08	0.17	0.42
P3	28fx x 1.8 Gy	0.83	0.85	0	1.37
P4	12fx x 4 Gy	-0.04	-0.04	0.52	0.46
P5 (Plan 1)	1fx x 18 Gy	0.04	0.04	0	0
P5 (Plan 2)	1fx x 20 Gy	0.55	0.49	0	0
Median		0.06	0.06	0	0.21
95th percent		0.75	0.74	0.41	1.10
Max.		0.83	0.85	0.52	1.37

Table 5: Differences in dose distributions of planning CT and Synthetic CT in the PTV, GTV, and two organs at risk structures, the brainstem and chiasma, for the different patients. P5 has received two plans for two different target volumes.

Conclusion of clinical Synthetic CT evaluation

In pelvis and brain, dosimetric errors were small and on average < 1% for target structures. Automated matching localization errors for pelvis were small and, on average, ~ 1 mm along each axis. For brain, they were not evaluated.

A potential limitation is that fiducials (and some calcifications) are generally converted to soft tissue, which precludes the ability to localize by fiducial when preferred or necessary. In the special case of prostate SBRT, for example, it would be desirable to have a fiducial-based localization methodology implemented.

However, a method to contour the fiducials and override the HUs in the Synthetic CT is available in the *syngo*.via RT Image Suite. This method was not evaluated in this clinical study.

In conclusion, the MR-based Synthetic CT solution provided a clinically appropriate level of dosimetric and spatial accuracy for standard fractionation cases. Overall, the Synthetic CT created by *syngo*.via RT Image Suite VB60[1] provides a clinically reasonable alternative to a CT simulation exam and may be used clinically in the treatment planning and treatment of prostate pelvic standard fractionation radiation therapy as well as for brain treatment planning.

[1] *syngo.via RT Image Suite VB60 and Synthetic CT is not commercially available in all countries. Its future availability cannot be guaranteed.*

Contributors

Michaela Hoesl, PhD
Global Product Marketing Manager

Nuria Escobar Corral, PhD
Global Product Marketing Manager

Nilesh Mistry, PhD
Product Manager
syngo.via RTiS

Xin Miao, PhD
MR Collaboration Scientist
Boston, USA

Clinical partners

Prof. Atchar Sudhyadhom, PhD
Medical Physicist
Brigham and Women's Hospital
Boston, USA

Siti Masitho
PhD student
Universitätsklinikum Erlangen, Germany

Prof. Christoph Bert, PhD
Chief Medical Physicist
Universitätsklinikum Erlangen, Germany

Florian Putz, MD
Radiation Oncologist
Universitätsklinikum Erlangen, Germany

Practical information

Software requirement	*syngo*.via RT Image Suite VB60 Deep learning-based Synthetic CT algorithm license
MRI scanner requirement and field strength	Training and testing were performed on a wide range of Siemens 1.5T and 3T MAGNETOM MRI scanners: MAGNETOM Aera, Skyra, Sola, Vida, Sola Fit The data acquisition protocols for Synthetic CT are available with *syngo* MR XA11A and later software versions for MAGNETOM RT Pro edition for MAGNETOM Vida and MAGNETOM Sola, with *syngo* XA30 and later software versions for MAGNETOM Aera and MAGNETOM Skyra.
In-plane resolution	1 mm x 1 mm brain 2 mm x 2 mm pelvis
Slice thickness	Slice thickness is controlled by the input slice thickness, determined by the acquired input T1 Vibe-Dixon sequence.
Geometric distortion	The 3D distortion is automatically selected for the sequences in the RT Dot Engine.
Algorithm training	• Trained with a fixed number of datasets during product development and locked at the time of release. The algorithm does not learn continuously in the field. • Updates do not take place automatically. • Training and validation images were randomly assigned from the data pool. • Brain: 6486 training image sets (CT + MR) and 553 validation sets • Pelvis: 9059 training image sets and 695 validation sets • Data augmentation of the original data has been performed.
MR-based Synthetic CT generation	The acquisition time at the scanner is limited to only one sequence: T1 VIBE Dixon. Acquisition times may vary between 1 min 33 s and 4 min 12 s depending on field strength, clinical site, and acceleration modes.

References

[1] R. W. Brown, Y.-C. N. Cheng, E. M. Haacke, M. R. Thompson, and R. Venkatesan, "Magnetic resonance imaging: physical principles and sequence design", John Wiley & Sons, 2014.

[2] R. Speight et al., "IPEM Topical Report: An international IPEM survey of MRI use for external beam radiotherapy treatment planning", Phys. Med. Biol., vol. 66, no. 7, 2021.

[3] G. P. Liney et al., "Quantitative evaluation of diffusion-weighted imaging techniques for the purposes of radiotherapy planning in the prostate", Br. J. Radiol., vol. 88, no. 1049, pp. 1–6, 2015.

[4] W. D. Foltz et al., "Readout-segmented echo-planar diffusion-weighted imaging improves geometric performance for image-guided radiation therapy of pelvic tumors", Radiother. Oncol., vol. 117, no. 3, pp. 525–531, 2015.

[5] D. Thorwarth, M. Notohamiprodjo, D. Zips, and A.-C. Müller, "Personalized precision radiotherapy by integration of multi-parametric functional and biological imaging in prostate cancer: a feasibility study", Z. Med. Phys., vol. 27, no. 1, pp. 21–30, 2017.

[6] C. Dinis Fernandes et al., "Quantitative 3T multiparametric MRI of benign and malignant prostatic tissue in patients with and without local recurrent prostate cancer after external-beam radiation therapy", J. Magn. Reson. Imaging, vol. 50, no. 1, pp. 269–278, 2019.

[7] M. A. Speight, Richard Dubec, Michael Eccles, Cynthia L George, Ben Henry, Ann Herbert, Trina Johnstone, Robert I Liney, Gary P McCallum, Hazel Schmidt, IPEM topical report: guidance on the use of MRI for external beam radiotherapy treatment planning. Physics in Medicine and Biology, 2021.

[8] K. K. Brock, "Adaptive Radiotherapy: Moving Into the Future", Semin. Radiat. Oncol., vol. 29, no. 3, pp. 181–184, 2019.

[9] K. Latifi, J. Caudell, G. Zhang, D. Hunt, E. G. Moros, and V. Feygelman, "Practical quantification of image registration accuracy following the AAPM TG-132 report framework", J. Appl. Clin. Med. Phys., vol. 19, no. 4, pp. 125–133, 2018 .

[10] QA cookbook: Commissioning and Quality Assurance (QA) for MAGNETOM systems in radiation therapy, siemens-healthineers.com/magnetom-world-rt 2021 HOOD05162003187576

[11] C. Tsien, Y. Cao, and T. Chenevert, "Clinical Applications for Diffusion Magnetic Resonance Imaging in Radiotherapy", Seminars in Radiation Oncology, 24(3), 218–226, 2014.

[12] M. A. Schmidt and G. S. Payne, "Europe PMC Funders Group Radiotherapy Planning using MRI", Phys. Med. Biol., vol. 60, no. 22, pp. R323–R361, 2015.

[13] E. Paradis, C. Yue, T. S. Lawrence, C. Tsien, K. Vineberg, and J. M. Balter, "Assessing the dosimetric accuracy of MR-generated synthetic CT images for focal brain VMAT radiotherapy Eric", Int J Radiat Oncol Biol Phys, vol. 93, no. 5, pp. 1154–1161, 2015.

[14] E. S. Paulson et al., "Consensus opinion on MRI simulation for external beam radiation treatment planning", Radiother. Oncol., vol. 121, no. 2, pp. 187–192, 2016.

[15] E. Johnstone et al., "Systematic Review of Synthetic Computed Tomography Generation Methodologies for Use in Magnetic Resonance Imaging–Only Radiation Therapy", Int. J. Radiat. Oncol. Biol. Phys., vol. 100, no. 1, pp. 199–217, 2018.

[16] L. Vandewinckele et al., "Overview of artificial intelligence-based applications in radiotherapy: Recommendations for implementation and quality assurance", Radiother. Oncol., 2020.

[17] C. K. Glide Hurst et al., "Task Group 284 Report: Magnetic Resonance Imaging Simulation in Radiotherapy: Considerations for Clinical Implementation, Optimization, and Quality Assurance", Med. Phys., 2021.

[18] J. M. Edmund and T. Nyholm, "A review of substitute CT generation for MRI-only radiation therapy", Radiat. Oncol., vol. 12, no. 1, pp. 1–15, 2017.

[19] D. A. Low et al., "A technique for the quantitative evaluation of dose distributions", Med Phys May; 25(5): 565-61, 1998.

On account of certain regional limitations of sales rights and service availability, we cannot guarantee that all products included in this brochure are available through the Siemens Healthineers sales organization worldwide.

Availability and packaging may vary by country and are subject to change without prior notice. Some/All of the features and products described herein may not be available in all countries.

The information in this document contains general technical descriptions of specifications and options as well as standard and optional features that do not always have to be present in individual cases.

Siemens Healthineers reserves the right to modify the design, packaging, specifications, and options described herein without prior notice. Please contact your local Siemens Healthineers sales representative for the most current information.

Note: Any technical data contained in this document may vary within defined tolerances. Original images always lose a certain amount of detail when reproduced.

The statements by Siemens' Healthineers customers described herein are based on results that were achieved in the customer's unique setting. Because there is no "typical" hospital or laboratory and many variables exist (e.g., hospital size, samples mix, case mix, level of IT and/or automation adoption) there can be no guarantee that other customers will achieve the same results.

Siemens Healthineers Headquarters
Siemens Healthcare GmbH
Henkestr. 127
91052 Erlangen, Germany
Phone: +49 9131 84-0
siemens-healthineers.com

Published by Siemens Healthcare GmbH · 11725 0322 online ·